



## Research Article

# Photo-assisted mineralisation of titan yellow dye using ZnO nanorods synthesised via environmental benign route



C. Vidya<sup>1</sup> · C. Manjunatha<sup>2,3</sup>  · M. Sudeep<sup>1</sup> · S. Ashoka<sup>4</sup> · M. A. Lourdu Antony Raj<sup>1</sup>

Received: 26 October 2019 / Accepted: 14 March 2020 / Published online: 21 March 2020

© Springer Nature Switzerland AG 2020

### Abstract

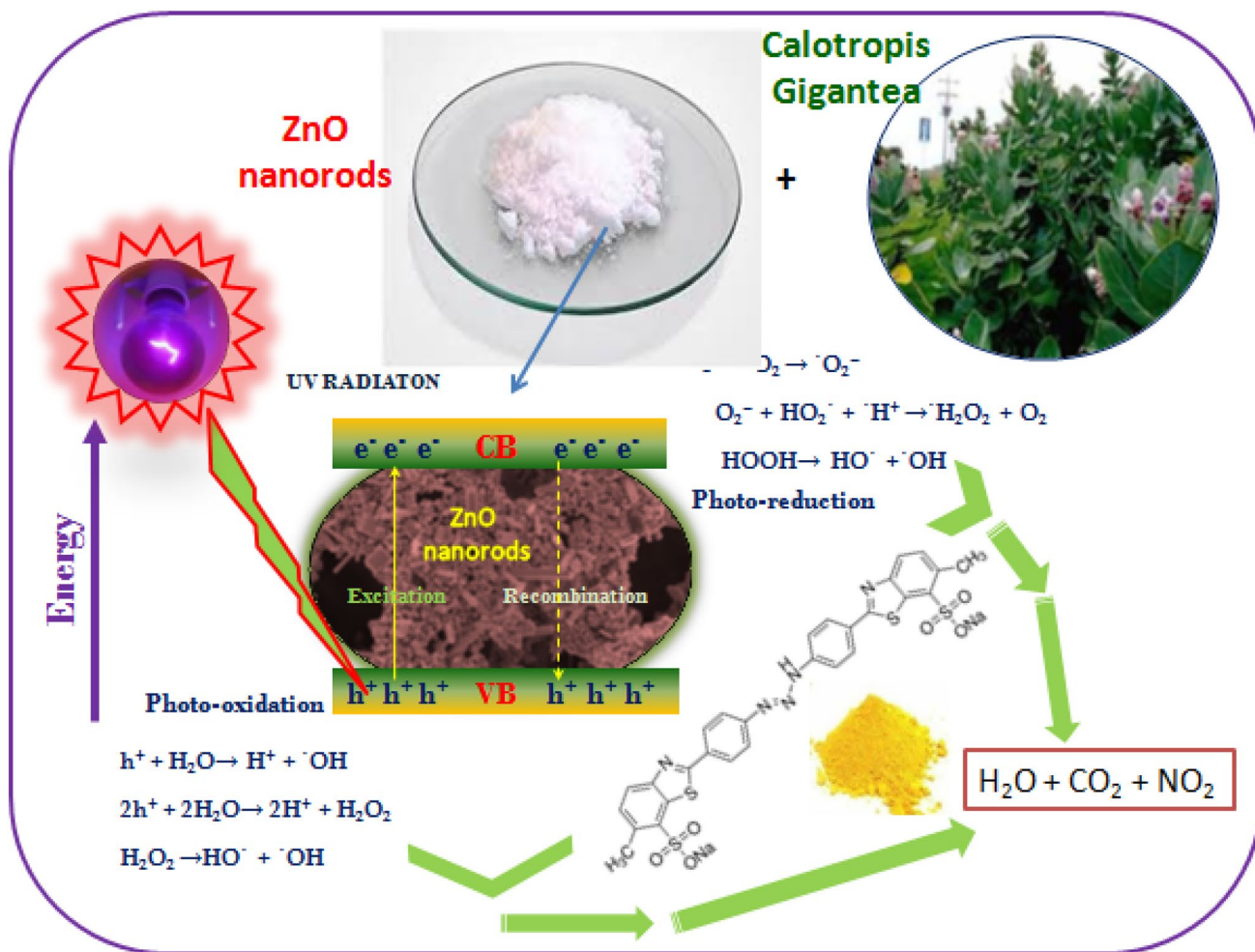
Green synthesis of metal oxide nanoparticles using plant extract is a most promising substitute for regular methods that involve chemical synthesis approach. The present study reports the synthesis of ZnO nano rods (ZNRs) using *Calotropis gigantea*, a plant rich in flavonoids and alkaloids and their application as a photocatalyst in the degradation of titan yellow dye. The synthesized ZNRs were characterized using XRD, FESEM–EDS and HRTEM–SAED. The XRD results confirm the formation of wurtzite ZnO. The FESEM images confirmed that ZNRs have length ranging from 20 to 200 nm, diameter ranging between 20 and 80 nm and width between 20 and 50 nm. The bio-synthesized ZNRs were used for photo-degradation of titan yellow dye, one of the main effluents from textile industries, discharged directly into water bodies. The ZNRs exhibited 95% dye degradation for 10 ppm TY dye concentration in the presence of 60 mg of the ZNRs catalyst at pH 8 for 60 min UV irradiation. The present study reports eco-friendly method for the synthesis of ZNRs and its efficiency as a photo catalyst in the advanced photo assisted oxidation process for degradation of titan yellow dye.

✉ C. Manjunatha, manjunathac@rvce.edu.in; manju.chem20@gmail.com | <sup>1</sup>Department of Chemical Engineering, R.V. College of Engineering, Bengaluru 560059, India. <sup>2</sup>Department of Chemistry, R.V. College of Engineering, Bengaluru 560059, India. <sup>3</sup>Visvesvaraya Technological University, Belagavi 590018, India. <sup>4</sup>Department of Chemistry, Dayananda Sagar University, Bengaluru 560068, India.



SN Applied Sciences (2020) 2:743 | <https://doi.org/10.1007/s42452-020-2537-2>

Graphic abstract



**Keywords** Green synthesis · ZnO nanorods · Titan yellow · *Calotropis gigantea* · Degradation

**1 Introduction**

Nowadays, the world environmental pollution especially due to water pollution, caused by organic contaminants has become a severe threat to humans and aquatic living beings. Since last decade, worldwide, many research groups are continuously researching to purify polluted water from its contaminants, major portion of which are organic in nature [1]. Textile industry is one of the main sources of water pollution worldwide because of its dye-containing effluents which are let into water bodies; attracting global concern. The waste water containing dye adversely affects the aquatic environment by impeding penetration of light and hence leads to an imbalance in the aquatic and dependent ecosystem. Added to this, the toxic and carcinogenic nature of most of these dyes

are threat to human health [2]. One such dye found in effluents from textile industries is titan yellow [3]. Degradation of dye molecules, owing to their harmful influences on human health and environment, becomes necessary. Reports suggest that degradation of these dyes sometimes results in the formation of non-coloured dye fragments which, although meet the requirement of decolourization satisfactorily, lead to the formation of environmentally unfriendly degradation products, such as aromatic amines, which are proven to be much more toxic than the parent dyes [4]. The decolourization and degradation of modern dye molecules, is ineffective by conventional biological treatment methods due to the stable nature and high levels of aromatics.

Physico-chemical methods such as coagulation/flocculation, adsorption by activated carbon and reverse osmosis

techniques have been developed to target the removal of dye in the discharged effluents [5]. Chemical techniques like ozonolysis, oxidation/reduction, decolorizes the effluent by altering the chemical structure of the dye but release several other by-products which accumulate in the water bodies [6]. Effluent treatment by biological techniques like aerobic/anaerobic digestion and electrochemical techniques like ion-oxidation result in sludge formation leading to an increase in the solid disposal cost [7]. Advanced oxidation process (AOP) in which the generated hydroxyl ions are used for treating the organic waste in the effluent has gained significant attention as a potential research area. Further, the process also enables the waste to be completely degraded to carbon dioxide, water and some inorganic ions. AOPs employ photo catalysts, fenton reagents, ozone, hydrogen peroxide, and ultraviolet or solar light, either independently or in a suitable combination [8] for the removal of dyes. AOP that utilizes metal oxides as photocatalysts for effluent treatment is a widely researched area [9].

Transition metal oxide nanoparticles like ZnO, TiO<sub>2</sub>, CeO<sub>2</sub>, SnO<sub>2</sub>, CuO-SnO<sub>2</sub>, Cu-TiO<sub>2</sub> are used as catalyst for photo degradation due to their ability of generating charge carriers when irradiated with UV/solar radiations [10–13]. Very few researchers have reported the degradation of titan yellow by photo catalysis using green synthesized ZnO. Studies on discoloration of direct yellow 9 by Elhbieta Regulska [14] using ZnO and TiO<sub>2</sub> nanoparticles report that ZnO photo degrades Direct Yellow 9 with twice the efficiency as compared to titanium dioxide. There are several reports on degradation of titan yellow dye using other photocatalysts such as TiO<sub>2</sub> [15],  $\alpha$ -Fe<sub>2</sub>O<sub>3</sub>,  $\gamma$ -Fe<sub>2</sub>O<sub>3</sub> [16].

ZnO as a semiconducting ( $E_g = 3.0$  eV) photocatalyst has been studied since 1935, due to its unique morphological structure, surface area and crystallinity [17], and explored its potential application as photo-catalyst and photovoltaic cells. The photo-catalytic behaviour of ZnO nanoparticles is mainly due to surface defects, oxygen vacancies, polar planes and surface area [18, 19]. Photo-generated holes in ZnO have strong oxidizing power to decompose most organic compounds. ZnO has often been considered as a valid alternative to TiO<sub>2</sub> because of its good optoelectronic, catalytic and photochemical properties combined with economic viability [10]. ZnO has a band gap of 3.0 eV that is lower than that of anatase TiO<sub>2</sub>, has been tested to decompose aqueous solutions of several dyes and many other environmental pollutants [20–22]. A wide range of novel ZnO nanostructures can be obtained by changing the growth conditions in the synthesis [23]. Studies on ZNRs structure have gained significance lately, and reports show that nano rods, offer higher surface to volume ratio compared to nano particulates.

Also studies have shown that one dimensional (1D) ZNRs arrays can significantly enhance photo-catalytic efficiency [24]. Nano assemblies, nano-plates, microspheres with nano-sheets and hierarchical ZNRs are widely used as nano-adsorbents for the removal of heavy metals from wastewater [25, 26]. These modified ZnO nanomaterials show higher photo-degradation efficiency due to their unique micro/nanostructure as compared to commercial ZnO [27, 28].

ZNRs are conventionally synthesized via chemical methods like precipitation, chemical vapour deposition, hydrothermal, solution combustion, sol-gel, sono and electrochemical methods [1, 29–31] which are actually not recommended in green chemistry. Biological approaches for synthesis of metal oxide nano particles have been suggested as valuable and eco-friendly alternatives to chemical methods [7].

Extensive research has been carried out on green mediated synthesis of metal oxides, sulphides and other various nanoparticles [32]. In green mediated synthesis, the ZnO nanoparticles are synthesized using biological sources such as plants leaves, flowers, fruits stem etc.[33–37]. In the present study, to the best of our knowledge, we report that ZNRs are green synthesised using water extract of *Calotropis gigantea* leaves for the first time. The detailed investigation on AOP for the mineralisation of titan yellow, one of the main constituents of effluents from textile industries, using ZNRs as photo catalysts is discussed.

## 2 Materials and methods

### 2.1 Materials

Zinc nitrate hexahydrate (Zn(NO<sub>3</sub>)<sub>2</sub>·6(H<sub>2</sub>O)) used for the experiments was of analytical grade and purchased from Merck Chemical Reagents Co. Ltd., India. Titan yellow (TY) dye was procured from Rolex Chemical Industries, India.

### 2.2 Synthesis of ZNRs using *Calotropis gigantea* leaves and zinc nitrate

Fresh leaves of *Calotropis gigantea* plant were collected from botanical garden of R V College of Engineering, Bengaluru, India. The collected leaves were washed thoroughly with deionised water to remove the dust particles and then dried in sun to remove the residual moisture. 50 g of washed, dried, cut and fine leaves were taken in 1000 ml glass beaker along with 500 ml of sterile distilled water. This mixture was then boiled to reduce the water content to 50% of its initial volume, which finally results into pale brown extract. The extract was then cooled to

room temperature, filtered and stored in a refrigerator for further experiments.

For the ZNRs synthesis, 100 ml of *Calotropis gigantea* leaves extract was taken and boiled at 60–80 °C using a magnetic stirrer with heating arrangement. When the temperature of the extract reached 80 °C, 5 g of Zinc nitrate hexahydrate ( $\text{Zn}(\text{NO}_3)_2 \cdot 6(\text{H}_2\text{O})$ ) was added and boiled to yield a deep yellow coloured paste. This paste was then collected in a ceramic crucible and calcined in muffle furnace at 400 °C for 1 h. The foam formed in the crucible was crushed in a mortar-pestle and stored in an air tight container for characterization and dye degradation studies.

### 2.3 Characterization techniques

Powder X-ray diffraction (PXRD) analysis was carried out by using CuK $\alpha$  radiations ( $k=1.54 \text{ \AA}$ ) on PXRD: JDX 8030, JEOL. The surface morphology and elemental analysis of green synthesized ZNRs were studied by the images captured using scanning electron microscope on Carl Zeiss Model: Neon-40 equipped with EDAX. The TEM observations were carried out with a JEOL 2000 FX-II microscope. For TEM characterization, the powder sample was dispersed in methanol by ultra-sonication for 20 min and loaded on copper grid. The FTIR studies were done on Model Thermo-Nicolet 6700 spectrometer. Diffuse reflectance UV–visible spectra were studied using Systronics double beam UV–visible Spectrophotometer.

### 2.4 Photo-catalytic activity

Photo catalytic degradation experiments were carried out in a photo reactor consisting of a circular glass vessel of 18 cm in diameter placed on a magnetic stirrer. The UV light source used in the dye degradation studies was Philips mercury vapour lamp of 30 W with a wavelength of 254 nm. The photon flux impinging on the reaction mixture was found to be 7.9 mW/cm<sup>2</sup> by ferri-oxalate-actinometric methods. All samples containing dye and photocatalyst to be irradiated were placed in the glass beaker and irradiated by focusing the light directly onto the reaction mixture at an irradiation distance of 23 cm.

For photo-catalytic degradation experiments, stock solutions of 1000 mg/L of titan yellow were prepared using double distilled water followed by dilution to obtain a series of dye solutions with varying concentrations. 250 ml of dye solution with a known amount of catalyst were taken in a glass vessel of 20 cm diameter, placed on a magnetic stirrer and irradiated. After irradiation around 5 ml of aliquot was drawn at regular intervals and allowed to settle to prevent the intervention of the catalyst. The rate of degradation of dye solution was assessed using spectrophotometer at a wavelength of 405 nm. The readings

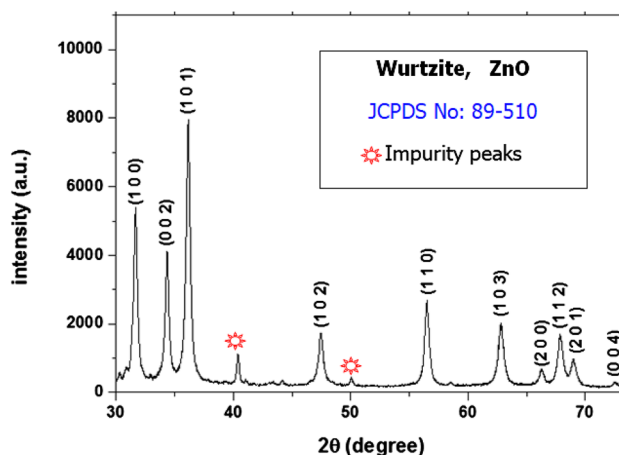


Fig. 1 XRD of green synthesised ZNRs

were noted down till the photo-degradation rate reached equilibrium. The degradation efficiency was determined using Eq. 1.

$$\% \text{ Photo degradation efficiency} = \frac{C_0 - C}{C_0} \times 100 \quad (1)$$

where  $C_0$  and  $C$  are initial and final dye concentrations respectively. The experiment was conducted to study the influence of various parameters such as pH, dye concentration and catalytic load on the dye degradation efficiency.

The synthesised ZNRs were added as a photocatalyst in a beaker containing 10–40 ppm TY solution. They were subjected to radiations from UV lamp by varying irradiation time and quantity of catalyst. The absorption spectra were recorded using JASCO V-570 UV–Vis spectrophotometer and rate of decolourization was studied.

## 3 Results and discussion

### 3.1 X-ray diffraction analysis

The structural characterization and phase identification of the synthesized ZNRs was performed by X-ray diffraction CuK $\alpha$  radiation in the  $2\theta$  range from 30° to 75°. Figure 1 shows the XRD peaks for ZNRs positioned at 31.66, 34.35, 36.17, 47.49, 56.51, 62.81, 66.29, 67.89, 68.99, 72.58 and can be indexed to [100], [002], [101], [102], [110], [103], [200], [112], [201] and [004] respectively. Results confirmed the presence of wurtzite structure which is similar to standard JCPDS No: 89-510 [1]. In the refinement of wurtzite ZnO with Zn at (1/3, 2/3, 0) and O at (1/3, 2/3, u), pseudo-voigt function has been taken into account in describing the Bragg shape (discussed in Sect. 3.4). The

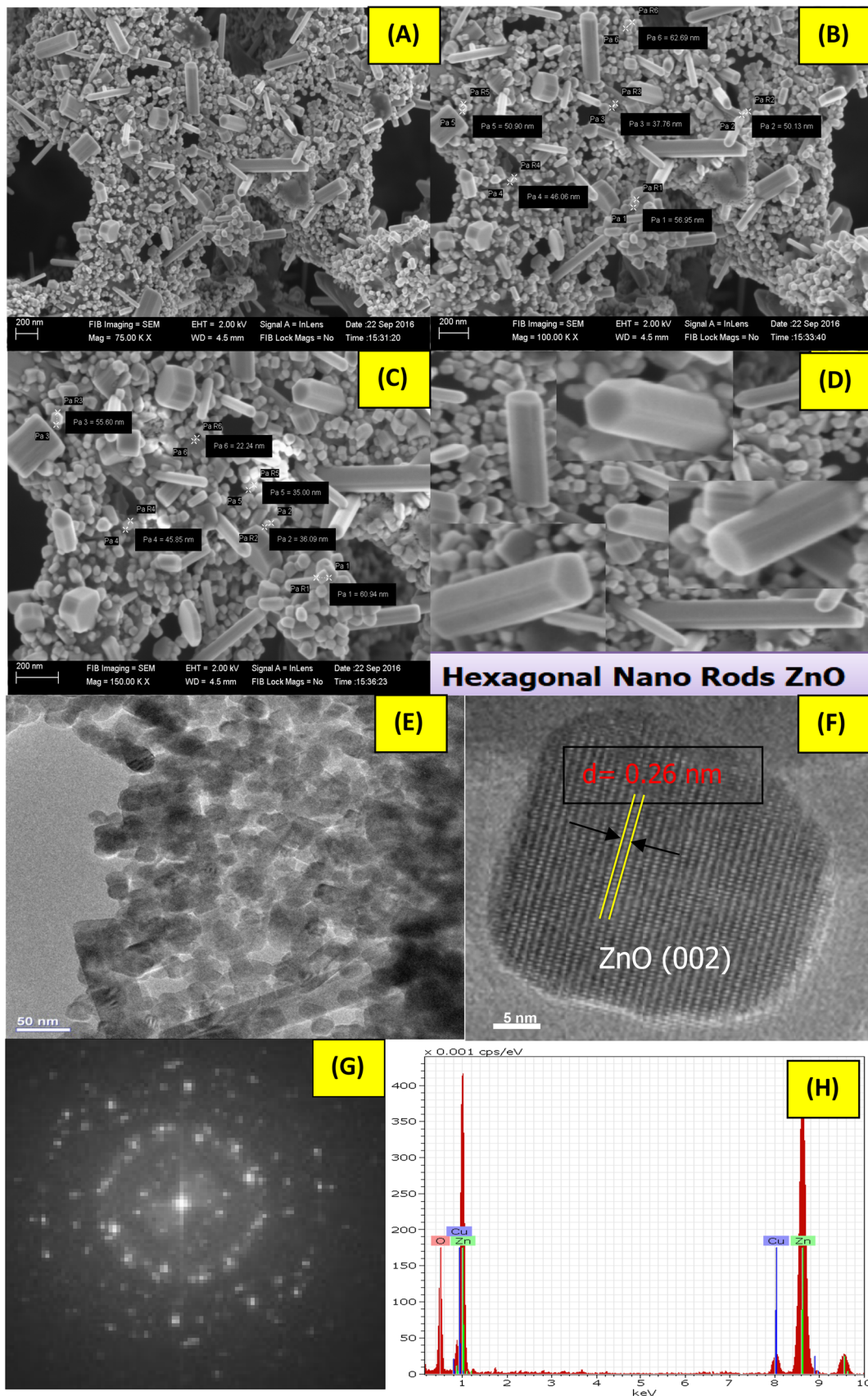


**Fig. 2** a–c FESEM images, d highly magnified FESEM images showing hexagonal ZNRs, e TEM, f HRTEM, g SAED and h EDS spectra ZNRs

additional peaks at  $2\theta = 42^\circ, 50^\circ$  is due to presence of trace amounts of impurity phases Zn,  $Zn(OH)_2$ , which is possible in green synthesis method using plant extracts.

### 3.2 ZNRs morphology analysis by FESEM, HRTEM, SAED and EDS

The FESEM was used to analyse the structural morphology of synthesised ZnO nanomaterials (Fig. 2). The SEM images indicate the presence of hexagonal nano-rods as seen in Fig. 2a, with length ranging between 20 and 200 nm, diameter ranging between 20 and 80 nm and width between 20 and 50 nm (Fig. 2b–d). This confirms that green mediated synthesis is a best suitable an environmentally benign route alternative to chemical methods for ZNRs. The TEM imaging was done to get an insight of morphology and size of ZNRs. After calcination from a conventional muffle furnace the ZnO nanoparticles tend to attain the shape of rods in hexagonal pattern. The TEM in Fig. 2e and HRTEM image in Fig. 2f confirms the formation of nano-rods and particles. The TEM images depicted in Fig. 2e show nanoparticles ranging between 20 and 40 nm which is in good agreement with the FESEM images. The HRTEM image also confirms the crystal lattice grown in the direction of (002) having 'd' spacing of 0.24 nm. The SAED pattern on ZNRs shown in Fig. 2g indicates that the ZnO is in poly crystalline in nature. From the EDS spectra shown in Fig. 2h it is evident that no impurities are present in the synthesized ZNRs as no peaks were observed for other substances

**Table 1** Refined parameters of synthesised ZNRs

Parameters	ZnO
Crystal structure	Hexagonal
Space group	P63mc (186)
Hall symbol	P 6c-2c
Lattice parameters (Å)	a = 3.2495, c = 5.2014
c/a	1.6
$\chi^2$	3.822
$R_p$	8.37
$R_{Bragg}$	2.04
$R_{exp}$	6.44
$R_{WP}$	10.3
GoF ( $R_{WP}/R_{exp}$ )	1.6
Volume of unit cell/formula unit (Å <sup>3</sup> )	47.5712
X-ray density (g/cm <sup>3</sup> )	5.702

which potentially amount to impurities. The 'Cu' peaks in EDS graph is due to the use of copper grid for TEM imaging. The elemental analysis showed the presence of zinc and oxygen in concentrations of 85.32% of and 14.68% respectively.

### 3.3 Rietveld refinement for ZNRs

Rietveld refinement method enables to precisely quantify different structure micro/nano structure parameters such as, lattice parameters, atomic coordinates and

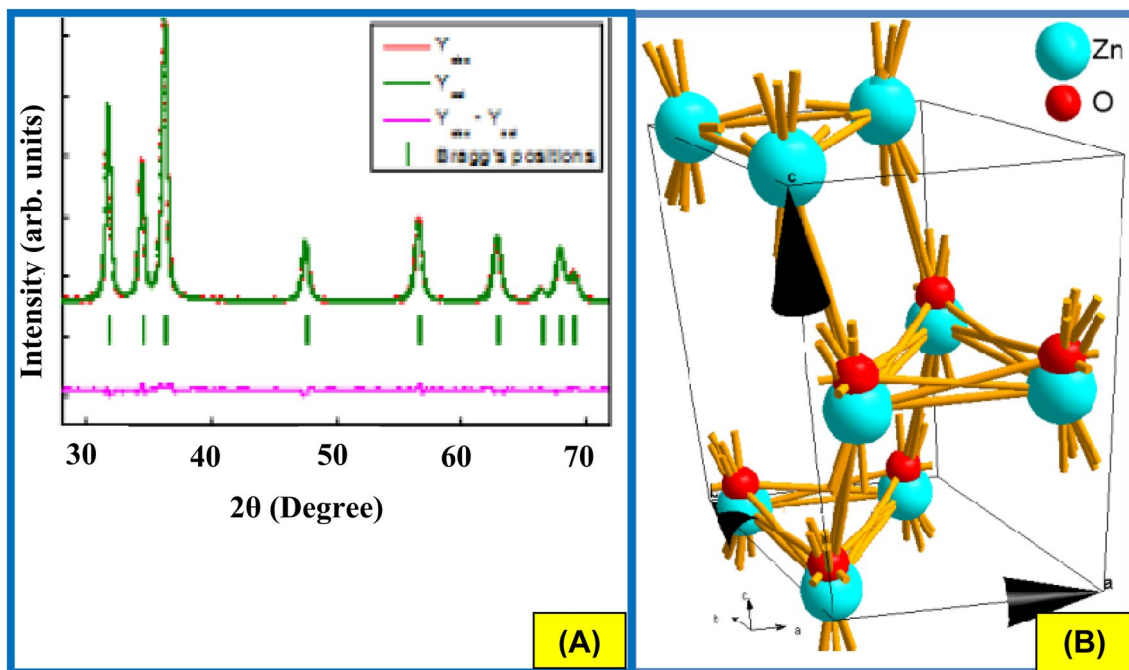


**Fig. 3** a Rietveld refinement b Packing diagram of ZNRs

occupancies, crystallite size, lattice strain etc. of any polycrystalline material to a good degree of precision using the readily available XRD data. The Rietveld refinement is a method of estimating and approximating the structural model for the real sample by using the profile intensities obtained from step-scanning measurements of the nanoparticles. The experimental and calculated PXRD pattern was obtained by the Rietveld refinement sample for ZNRs as shown in Fig. 3a. The refinement was done with the Full Prof (FP) free available software with a modified version of Thompson–Cox–Hastings pseudo-Voigt (TCHZ) function profile. Rietveld method utilizes the least-squares refinement for obtaining the best fit between the experimental data and the calculated data pattern based on the simultaneously refined models. The vertical lines below stand for the Bragg reflection positions for all possible patterns. The lower solid line shows the divergence of observed intensities from the calculated intensities. The various reliability parameters that reveal the fitting quality of experimental data and lattice constants are listed in Table 1. Values obtained were found to be consistent as reported in literature [38]. The fitting parameters ( $R_p$ ,  $R_{wp}$ , and  $\chi^2$ ) indicate a good correspondence between the refined and observed PXRD patterns. The quality of the refined data was checked by measuring goodness of fit (GOF) defined by Eq. 2.

$$\text{GOF} = \frac{R_{wp}}{R_{exp}} \quad (2)$$

The GOF for the synthesised nanoparticles was 1.6 which confirms good fitting of experimental and theoretical plots. Further we calculated  $c/a$  and wurtzite parameter  $u$ , which is defined as the relative displacement between Zn and O sub-lattices along the  $c$ -axis  $c/a$  and

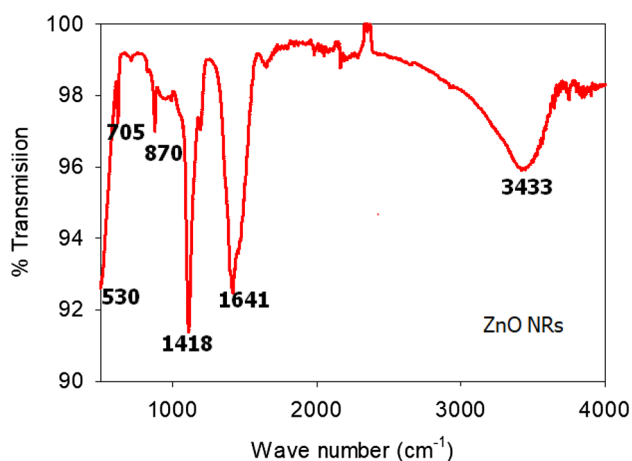


Fig. 4 FTIR spectra of green synthesized ZNRs

$u$  parameters as 1.6 and 0.375, respectively are in good agreement with the standard values for the bulk ZnO [39]. Diamond software was used to extract the possible packing diagram shown in Fig. 3b with space group P63mc. The lattice parameters  $a=b=3.24 \text{ \AA}$  and  $c/a=1.6 \text{ \AA}$  are in good agreement with (PCPDF No, 89-0510). From the packing diagram, the bond length between the neighbouring Zinc atoms was found to be  $3 \text{ \AA}$  and that between Zinc and Oxygen was found to be  $1.2136 \text{ \AA}$ .

The Lattice Parameters ( $\text{\AA}$ )  $a=3.2495$ ,  $c=5.2069$  with  $c/a=1.600$ ,  $V(\text{\AA}^3)=47.5712$  confirm the hexagonal wurtzite structure with GOF 1.6.

### 3.4 FTIR analysis of ZNRs

FTIR spectra (Fig. 4) for ZNRs show absorption band spectra below  $1000 \text{ cm}^{-1}$  due to inter atomic metal–oxygen vibrations. The peaks obtained at  $3433$ ,  $1418 \text{ cm}^{-1}$  can be accounted to stretching of O–H bond of surface adsorbed molecules. The stretching of respective bonds is attributed to the adsorption of water molecules onto the metal oxide nanoparticles. The characteristic absorption bands of metal oxides are generally observed below  $1000 \text{ cm}^{-1}$ , in their fingerprint region, arising from inter-atomic vibrations of metal and O ions. The peaks at  $1641$ ,  $705$  and  $530 \text{ cm}^{-1}$  correspond to Zn–O deformational vibrations [40]. The slight variation in the FT-IR peak position is attributed to changes in the crystallinity, surface purity, particle shapes and sizes.

### 3.5 Band gap energy calculations for ZNRs

Optical reflectance properties of the green synthesized ZNRs were analysed by recording UV diffuse reflectance between 200 and 800 nm. The band gap energy is calculated from Kubelka–Munk relation below:

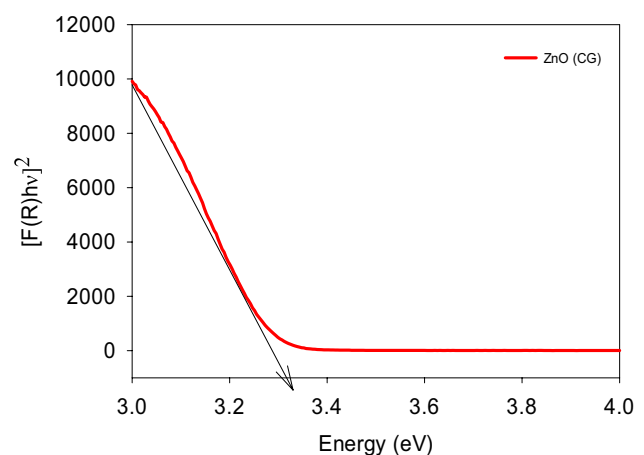


Fig. 5 Band gap energy for ZNRs

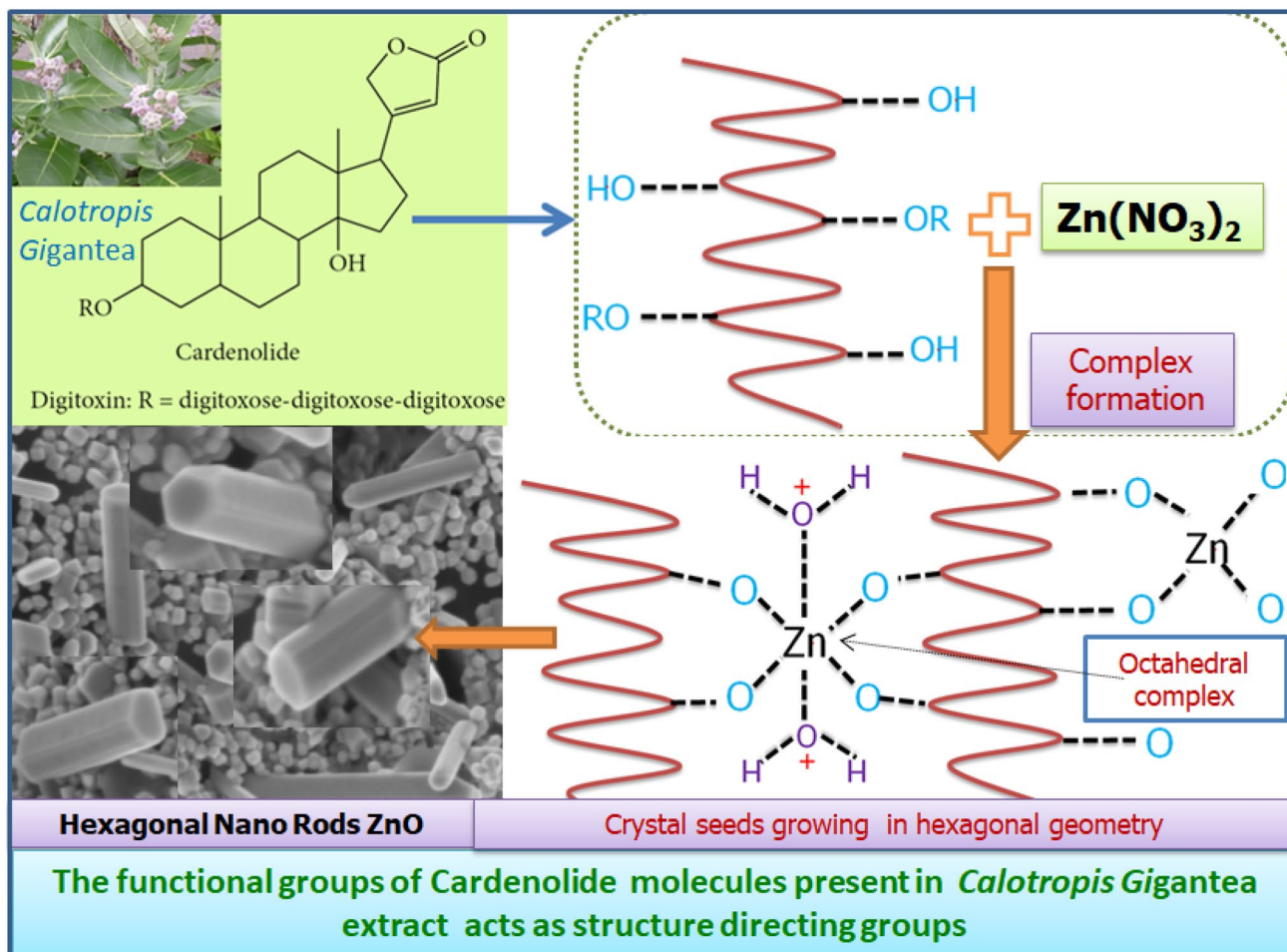


Fig. 6 Chemical structure of cardenolide glycosides of CG leave extract and plausible mechanism for the formation of ZNRs

$$F(R_{\infty})h\nu = C(h\nu - E_g)^n \tag{3}$$

$$R_{\infty} = \frac{R_{\text{Sample}}}{R_{\text{Standard}}}$$

R<sub>standard</sub>: 0.973–0.988 (BaSO<sub>4</sub> was taken as standard)

$$F(R_{\infty}) = \frac{(1 - R_{\infty})^2}{2R_{\infty}} = \frac{k}{s} \tag{4}$$

where hν: Photon energy (eV), F(R<sub>∞</sub>): Kubelka–Munk function, [F(R<sub>∞</sub>)/hν]<sup>2</sup>: Modified Kubelka–Munk function, k: the molar absorption coefficient and s: the scattering coefficient.

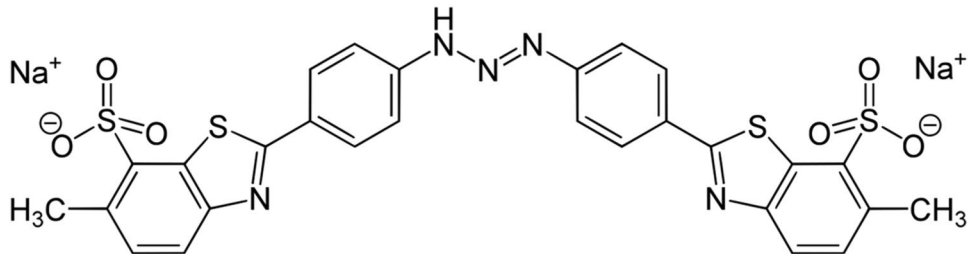
Strong maximum reflectance is observed above 375 nm. The band gap energy is found to be 3.31 eV (Fig. 5) for synthesised ZNRs and matches with the band gap reported for ZNRs [1].

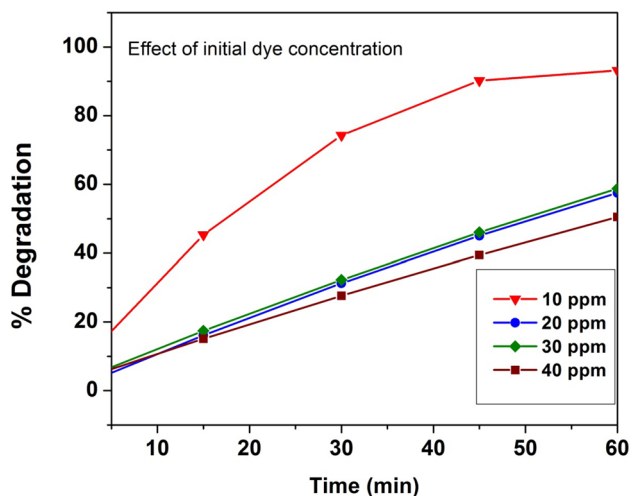
### 3.6 Plausible mechanism for the biogenic synthesis of ZNRs.

The plausible reaction mechanism of formation of ZnO nanorods is shown in Fig. 6. *Calotropis gigantea* (C.G) leaves extract mainly contains 19-Nor- and 18, 20-Epoxy-cardenolides along with flavonol glycosides, and cardiac glycoside, ursane triterpenes, cardenolides, and phytoosterols [41–43]. These organic molecules mainly contain hydroxyl, carbonyl and alkoxy functional groups as shown Fig. 6. During the green synthesis, Zn(NO<sub>3</sub>)<sub>2</sub>·6H<sub>2</sub>O mixed with C. G. leaf extract, the Zn<sup>2+</sup> ions distribute uniformly and form an octahedral complex with active sites of hydroxyl groups. When the formed complex of Zn<sup>2+</sup> and functional groups of cardenolides is subjected to calcination, the complex undergoes thermal decomposition leading to formation of zinc oxide. During thermal decomposition, polyphenolic molecules that interact with divalent Zn<sup>2+</sup> cations, which are bridged between four oxide and H<sub>2</sub>O molecules from two different chains



**Table 2** Structural features and properties of titan yellow

Properties of titan yellow	
Chemical formula	$C_{28}H_{19}N_5Na_2O_6S_4$
IUPAC name	Disodium 2,2'-[[1E]-triaz-1-ene-1,3-diyl]dibenzene-4,1-diyl]bis(6-methyl-1,3-benzothiazole-7-sulfonate)
Structure	
CI name/CI number	Direct yellow 9 19,540
Molar mass	695.720 g/mol
$\lambda_{max}$	398–405 nm
Type of dye	Anionic dye, triazine dye

**Fig. 7** Effect of initial TY dye concentration on ZNRs degradation efficiency

comes from polyphenolic group. The divalent cations keep the molecules together and form various structures of zinc complex [44]. The formation of octahedral complex helps in the crystal growth in hexagonal rod shapes, which is directed by functional groups of polyphenolic molecules of leave extract.

### 3.7 Photo degradation studies

Photo degradation of titan yellow dye was studied by investigation of parameters such as catalyst loading, dye concentration and pH. The structural features and properties of titan yellow are represented in Table 2. Dye

solutions of 10, 20, 30 and 40 ppm were prepared from 1000 ppm stock solution. The degradation was studied at room temperature by irradiating the dye solutions under UV light (254 nm). On the basis of these studies the kinetics of the photo-catalytic degradation was evaluated. The kinetic data was then analysed and fit to give the best Kinetic model.

#### 3.7.1 Effect of initial dye concentration

The effect of initial dye concentration was studied on 250 ml of 10, 20, 30, and 40 ppm dye solution at 60 mg of ZnO photocatalyst loading and pH of 8. It was found that the percentage of degradation is strongly influenced by the initial dye concentration and is > 90 for 10 ppm whereas 20, 30 and 40 ppm dyes recorded 50 and 60% degradation respectively (Fig. 7). Titan yellow is an azo dye, therefore the increase in dye concentration results in high hydrophobic interactions between aromatic rings resulting in the formation of aggregates that deposit on to catalyst surfaces thereby reducing the activity of the available catalyst surface. Since the number of hydroxyl radicals released by the catalyst surface to oxidise the dye molecules are less, hence the degradation percentage decreases. Moreover, this can be explained by the fact that less adsorption sites were being covered at lower dye concentrations; hence maximum photo-catalytic activity was recorded. Besides, lower initial concentrations leads to an increase in the affinity of the titan yellow dye towards the active sites. The decline in the adsorption capacity is due to the availability of smaller number of surface sites on the adsorbent for a relatively larger number of adsorbing species at lower concentrations.

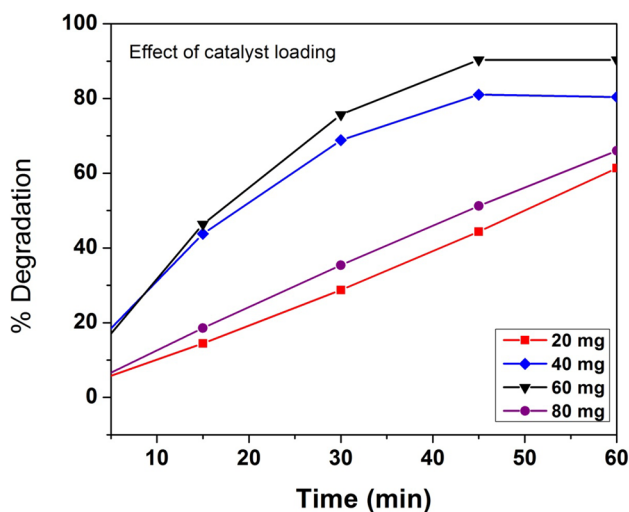


Fig. 8 Effect of ZNRs photocatalyst loading on TY dye degradation

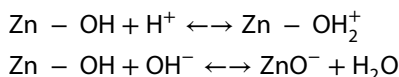
### 3.7.2 Effect of catalyst loading on degradation

The amount of catalyst is an important factor in adsorption method because it influences the recovery directly. Compared to ordinary sorbents (micro-sized sorbents), nanoparticles have higher surface areas. For this reason, fewer amounts of the adsorbent may achieve acceptable results because a significantly higher surface area-to-volume ratio. The influence of catalyst loading on degradation efficiency was studied on 250 ml of 20 ppm dye solution at a loading of 20, 40, 60 and 80 mg. The degradation was monitored for an hour at room temperature at a slightly alkaline pH of 8. It was seen that the degradation increased with the increase in catalyst loading up to 60 mg but gradually decreased with further increase in loading as shown in Fig. 8. The increase in the rate of dye degradation with increase in catalyst loading is due to formation of more and more hydroxyl free radicals. It is well documented observation for many dye degradation studies reported for ZnO photocatalyst. The formation of mechanism of formation hydroxyl free radicals is systematically discussed by several reports [33]. Chakrabarti have proved that, in the presence of a dye-sensitizer, a set of reactions in presence of water molecules and dissolved oxygen leading to the formation of several active oxygen species such as superoxide anion, singlet oxygen, hydroperoxyl radical besides hydroxyl radical [45]. Optimum catalyst loading was recorded to be 0.24 g/l for 20 ppm dye. The rate of degradation is related to the catalyst surface exposed to UV irradiation for the generation of electron-hole pair, which in turn generates hydroxyl radicals. It is plausible that with higher dosage of adsorbent, would result into greater availability of exchangeable active sites from dye. With the increase in amount of catalyst, the collision

between the particles increases, leading to the formation of more and more active sites. The high catalyst loading also induces opacity to the solution leading to decrease in the photo flux and hence reduces the rate of degradation. The decrease in adsorption capacity with the increasing of catalyst dosage may be due to the overlapping of the adsorption sites as a result of overcrowding of adsorbent particles. Moreover, the high adsorbent dosage could impose a screening effect of the dense outer layer of the cells, thereby shielding the binding sites from dye.

### 3.7.3 Effect of pH

The effect of pH on degradation was evaluated at room temperature for 1 h. The pH was varied from 6 to 10 with an increment of 2. Figure 9 shows the effect of pH on photo-catalytic degradation of TY dye. It was observed that the degradation rate increased as the pH was increased from 6 to 8 but showed a decrease at pH 10. The zero point discharge value (zpc) for ZnO is 9 [46]. There are three different reaction mechanisms which contribute to dye degradation, (1) Attack by hydroxyl radical, (2) Direct oxidation by the positive hole on the valence band, and (3) Direct reduction by the electron in the conduction band. The pH of the solution alters the electrical double layer of the metal oxide and dye solution interface. This affects the adsorption/desorption phenomena and separation of the photo-generated electron-hole pairs from the surface of the semiconductor particles. The pH is related to the ionization state of the surface in the following way:



The photocatalyst surface is positively charged when  $\text{pH} < \text{pH}_{\text{zpc}}$  where as it is negatively charged when  $\text{pH} > \text{pH}_{\text{zpc}}$ . This phenomenon strongly affects the adsorption and degradation process. The ZnO nanoparticles exhibit the zero point charge ( $\text{pH}_{\text{zpc}}$ ) of  $9.0 \pm 0.3$ . Therefore the ZnO catalyst surface is positively charged in acidic and slightly alkaline media ( $\text{pH} < 9$ ) whereas it is negatively charged under alkaline condition ( $\text{pH} > 9$ ) [47]. The degradation is found to be maximum for anionic dyes in acidic conditions, where as it is maximum for cationic dyes in alkaline condition. Since titan yellow is an anionic dye, it should be strongly attached to the positively charged photocatalyst surface. However, photo-catalytic degradation efficiency of ZnO was observed to be the highest at alkaline pH, even though the adsorption of titan yellow should be lower at this pH. The possible reason for the observed behaviour could be that in alkaline pH, where a large amount of hydroxyl ions are present, which directly

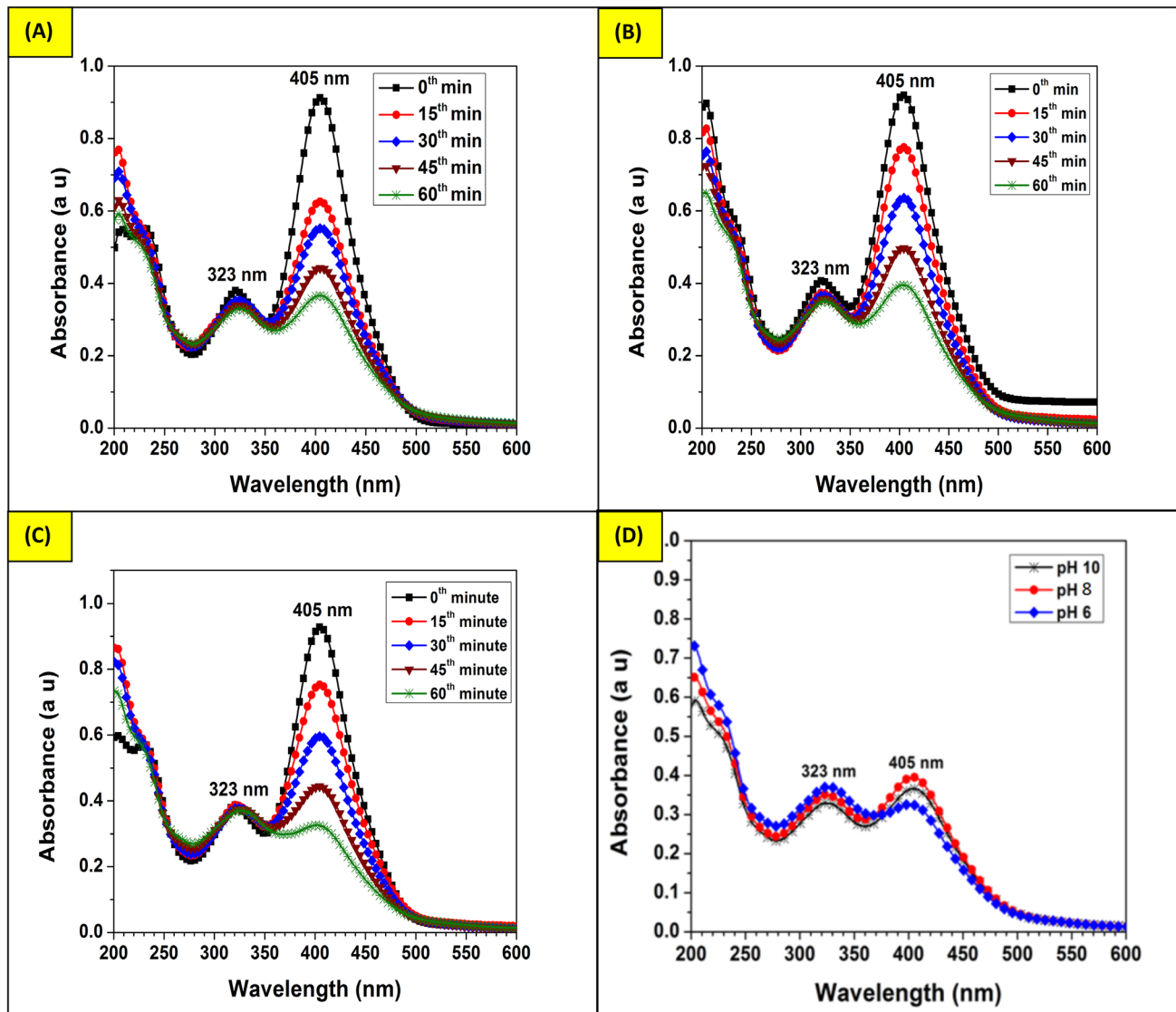


Fig. 9 Effect of pH tested at **a** pH 6, **b** pH 8, **c** pH 10, **d** consolidated pH after 60 min on ZNRs photocatalyst degradation efficiency

attacks on dye liberating highly active free radicals are favourably created and can significantly enhance the photo-catalytic degradation of a dye. At a given pH, the degradation of dye is also depending on the pKa value of dye molecule. It is very well known fact that higher the pKa value of a compound, lower is its pH and vice versa. In general, for ZnO photo catalyst, the optimum photo-degradation efficiency was observed at  $pK_a < pH < pHzpc$ . The increase in degradation efficiency with increase in pH is due to the formation of superoxide anion, singlet oxygen, hydroperoxyl radical, hydroxyl radical etc. During degradation reaction in the presence of UV light, many factors influence the degradation reaction. It is very difficult to explain the increase in degradation efficiency of ZnO photo catalyst surface charge. The intermediates products

formed, pH, reactive free radicals all will influence degradation reaction.

### 3.7.4 Photo-degradation mechanism and kinetics

The detailed mechanism of the ZNRs photocatalyst is schematically illustrated in Fig. 10. When ZNRs photo catalyst is irradiated by UV light possessing the energy equal to or greater than the ZnO band gap, a photo-electron moves from valence band (VB) of ZnO to the empty conduction band (CB). Thus a hole is created in VB ( $h_{VB}^+$ ) and an electron ( $e_{CB}^-$ ) in CB generated as shown in Fig. 10. The hole formed in the VB, further reacts with  $H_2O$ , then produce  $OH^*$  free radical, which act as a powerful oxidising agent and oxidise adsorbed organic dye molecules which are in

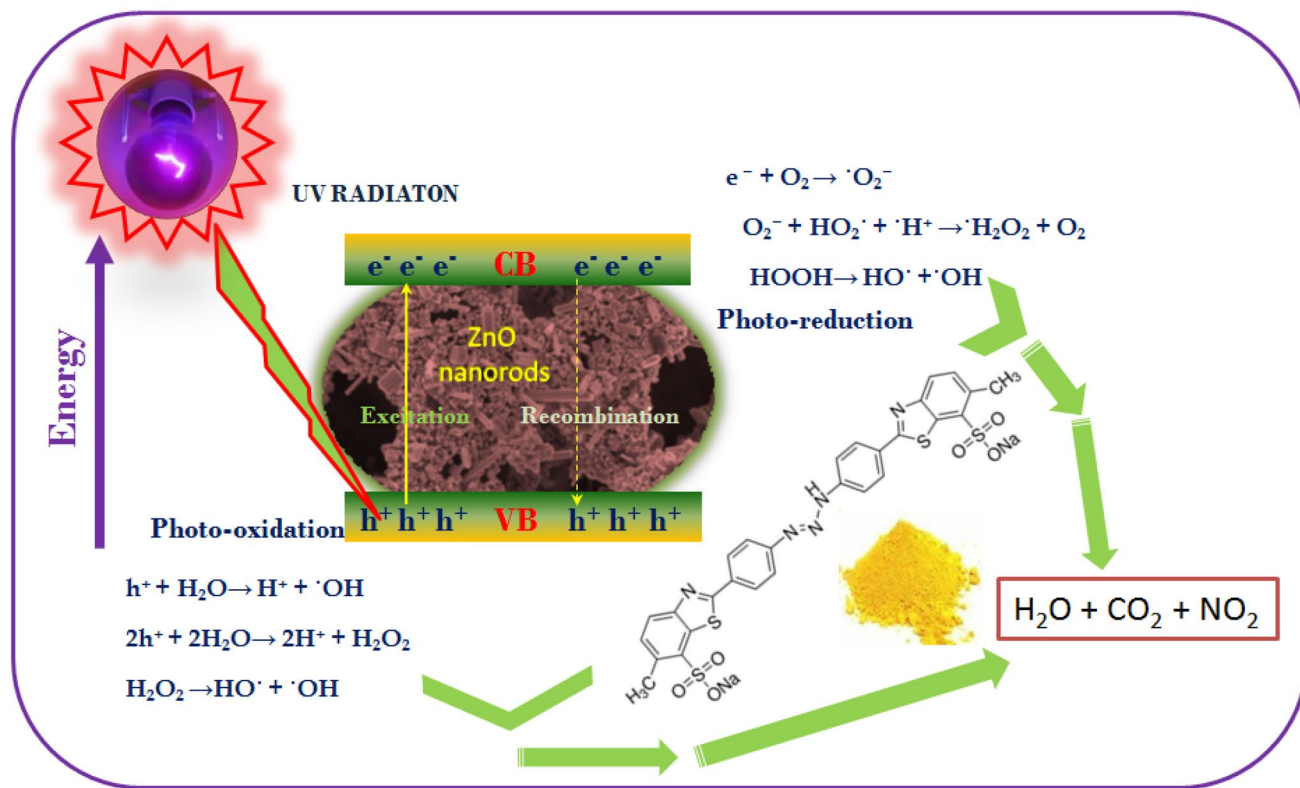


Fig. 10 Schematic representation of mechanism of photo-catalysis of ZNRs

near vicinity of ZNRs surface. Meanwhile, the electrons in (e<sub>CB</sub><sup>-</sup>) CB, reacts with O<sub>2</sub> and produce superoxide radicals (O<sub>2</sub><sup>-\*</sup>), which increase the speed of oxidation process. The superoxide radicals also prevent electron–hole recombination and helps in maintaining electrical neutrality in ZnO. During the degradation reaction, O<sub>2</sub><sup>-\*</sup> super oxide, further reacts with H<sup>+</sup> formed in reaction. The protonated hydroperoxyl radical (HO<sub>2</sub><sup>-\*</sup>), ultimately produces highly reactive hydroxyl radical (OH<sup>\*</sup>). The generated OH<sup>\*</sup> radicals constantly attack the TY dye structure at different sites like N=N groups, 'S' atoms, un-saturation points etc. During the constant attack of OH<sup>\*</sup> radicals, the TY dyes get mineralized into H<sub>2</sub>O, CO<sub>2</sub> which are stable, hazard free products [48].

The kinetics of the photo-catalytic degradation of organic dyes usually follows the Langmuir–Hinshelwood mechanism [49]:

$$r = -\frac{dC}{dt} = \frac{K_1 K_2 C}{1 + K_2 C_0} = K_{app} C \quad (5)$$

where r is the rate of disappearance of dye (mg/l/min), C is the concentration of the reactant (mg/l), K<sub>1</sub> is the surface reaction rate constant (mg/l/min), K<sub>2</sub> is the Langmuir Hinshel wood adsorption equilibrium constant of the reactant

(l/mg). Integration of Eq. (5) (with the restriction of C=C<sub>0</sub> at t=0) will lead to the following relation:

$$\ln \frac{C_0}{C} = K_1 K_2 t = K_{app} t \quad (6)$$

where K<sub>app</sub> is the pseudo first-order rate constant determined by the slope of the graph of ln(C<sub>0</sub>/C) versus t, where C<sub>0</sub> is the initial concentration of the reactant and C is the concentration at any time t. A plot of ln(C<sub>0</sub>/C) versus t is shown in Fig. 11. A linear expression can be conventionally obtained by plotting the reciprocal initial rate constant against initial concentration:

$$\frac{1}{K_{app}} = \frac{1}{K_1 K_2} + \frac{C}{K_1} \quad (7)$$

The kinetic studies for the degradation of titan yellow dye very well fit the Langmuir Hinshelwood kinetics. The corresponding kinetics plot of TY by ZNRs photo-catalysis under UV-irradiation for different dye concentration, photocatalyst loading and different pH are represented in Fig. 11.

The degradation of dyes fits L–H kinetics with an average rate constants found to be 35, 37 and 40 min<sup>-1</sup> for

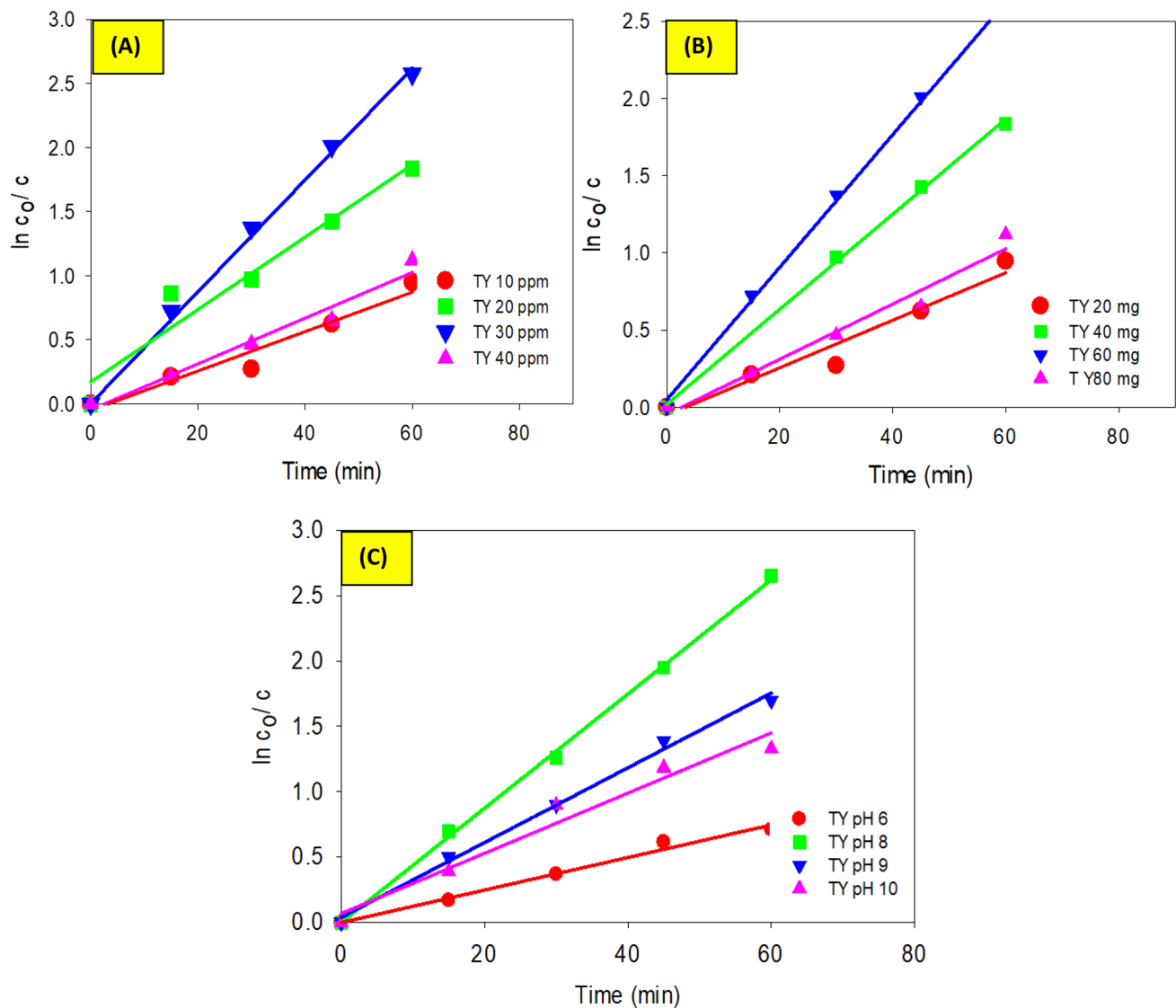


**Fig. 11** Langmuir–Hinshelwood kinetics plot of TY by ZNRs photocatalyst under UV-irradiation; **a** TY dye concentration, **b** photocatalyst loading and **c** pH

different catalyst loading, dye concentration and pH respectively.

#### 4 Conclusion

The hazard free, biodegradable *Calotropis gigantea* leaves extract as a reactant precursor for conversion of zinc nitrate hexahydrate into hexagonal shaped nano rods of ZnO is presented. The green synthesised ZNRs have been employed in degradation of titan yellow in the presence of UV light to study their photo-catalytic behaviour. The degradation efficiency of ZNRs photocatalyst is been carried out at various catalyst loading, pH, and for different TY dye concentration. More than 95% TY dye degradation

was achieved for 10 ppm dye concentration using 60 mg of the ZNRs catalyst load at pH of 8. The kinetics study of dye degradation reaction reveals that the photocatalytic reaction is in accordance with Langmuir Hinshel Wood Kinetics with an average rate found to be 35, 37 and 40  $\text{min}^{-1}$  for different catalyst loading, dye concentration and pH respectively. Over all the results suggests that, the leave extract of *Calotropis gigantea* plant could be very promising reactant precursor for hazard free wet chemical synthesis of ZnO nanoparticles and the same can be employed for also for synthesis for many other semiconducting nanostructured photocatalyst. The ZNRs prepared in our work, could also be used as a potential photocatalyst for the degradation other environmentally

hazard dyes, organic compounds and for adsorption toxic metal ion.

**Acknowledgements** This research did not receive any specific grant from funding agencies in the public, commercial, or not-for-profit sectors. However, Authors are grateful to Management of Raash-treeya Sikshana Samithi Trust (RSST) and the Principal, HOD Chemical Engineering, HOD Chemistry of R. V. College of Engineering,, Bengaluru, India for encouraging, supporting.

## Compliance with ethical standards

**Conflict of interest** The authors declare that they have no conflict of interest.

## References

- Jena M, Manjunatha C, Shivaraj BW, Nagaraju G, Ashoka S, Sham Aan MP (2019) Optimization of parameters for maximizing photocatalytic behaviour of  $Zn_{1-x}Fe_xO$  nanoparticles for methyl orange degradation using Taguchi and Grey relational analysis approach. *Mater Today Chem* 12:187–199
- Gonçalves MST, Pinto EMS, Nkeonye P, Oliveira-Campos AMF (2005) Degradation of C.I. Reactive Orange 4 and its simulated dyebath wastewater by heterogeneous photocatalysis. *Dyes Pigments* 64(2):135–139
- Yaseen DA, Scholz M (2019) Textile dye wastewater characteristics and constituents of synthetic effluents: a critical review. *Int J Environ Sci Technol* 16(2):1193–1226
- Mani P, Fidal VT, Bowman K, Breheny M, Chandra TS, Keshavarz T, Kyazze G (2019) Degradation of azo dye (Acid Orange 7) in a microbial fuel cell: comparison between anodic microbial-mediated reduction and cathodic laccase-mediated oxidation. *Front Energy Res* 7(101):1–12
- Rauf MA, Ashraf SS (2009) Fundamental principles and application of heterogeneous photocatalytic degradation of dyes in solution. *Chem Eng J* 151(1):10–18
- Kitanosono T, Masuda K, Xu P, Kobayashi S (2018) Catalytic organic reactions in water toward sustainable society. *Chem Rev* 118(2):679–746
- Vidya C, Prabha MNC, Raj MALA (2016) Green mediated synthesis of zinc oxide nanoparticles for the photocatalytic degradation of Rose Bengal dye. *Environ Nanotechnol Monit Manag* 6:134–138
- Cheng M, Zeng G, Huang D, Lai C, Xu P, Zhang C, Liu Y (2016) Hydroxyl radicals based advanced oxidation processes (AOPs) for remediation of soils contaminated with organic compounds: a review. *Chem Eng J* 284:582–598
- Muhd Julkapli N, Bagheri S, Bee Abd Hamid S (2014) Recent advances in heterogeneous photocatalytic decolorization of synthetic dyes. *Sci World J* 2014:692307–692307
- Ani IJ, Akpan UG, Olutoye MA, Hameed BH (2018) Photocatalytic degradation of pollutants in petroleum refinery wastewater by  $TiO_2$ - and  $ZnO$ -based photocatalysts: recent development. *J Clean Prod* 205:930–954
- Xia H-L, Zhuang H-S, Zhang T, Xiao D-C (2007) Photocatalytic degradation of Acid Blue 62 over  $CuO-SnO_2$  nanocomposite photocatalyst under simulated sunlight. *J Environ Sci (China)* 19:1141–1145
- Kumar M, Murugadoss G, Pirogov A, Rangasamy T (2018) A facile one step synthesis of  $SnO_2/CuO$  and  $CuO/SnO_2$  nanocomposites: photocatalytic application. *J Mater Sci Mater Electron* 29:13508–13515
- Mishra G, Mukhopadhyay M (2019)  $TiO_2$  decorated functionalized halloysite nanotubes ( $TiO_2@HNTs$ ) and photocatalytic PVC membranes synthesis, characterization and its application in water treatment. *Sci Rep* 9(1):4345
- Regulska E, Brus DM, Rodziewicz P, Sawicka S, Karpinska J (2016) Photocatalytic degradation of hazardous Food Yellow 13 in  $TiO_2$  and  $ZnO$  aqueous and river water suspensions. *Catal Today* 266:72–81
- Hiremath S, Mal AR, Prabha C, Vidya C (2018) Tamarindus indica mediated biosynthesis of nano  $TiO_2$  and its application in photocatalytic degradation of Titan yellow. *J Environ Chem* 6(6):7338–7346
- Akrami A, Niazi A (2016) Synthesis of maghemite nanoparticles and its application for removal of Titan yellow from aqueous solutions using full factorial design. *Desalin Water Treat* 57(47):22618–22631
- Ong CB, Ng LY, Mohammad AW (2018) A review of  $ZnO$  nanoparticles as solar photocatalysts: synthesis, mechanisms and applications. *Renew Sustain Energy Rev* 81:536–551
- Tan ST, Umar AA, Salleh MM (2016) Synthesis of defect-rich, (001) faceted- $ZnO$  nanorod on a FTO substrate as efficient photocatalysts for dehydrogenation of isopropanol to acetone. *J Phys Chem Solids* 93:73–78
- Reshak A, Tan ST, Naumar FY, Umar A, Oyama M, Alahmed Z, Kamarudin H, Kityk I (2014) Photoinduced nonlinear optical second-order optical effects in the  $Ag-ZnO$  nanorods. *Int J Electrochem Sci* 9:6352–6358
- Jiang L, Yuan X, Zeng G, Wu Z, Liang J, Chen X, Leng L, Wang H, Wang H (2018) Metal-free efficient photocatalyst for stable visible-light photocatalytic degradation of refractory pollutant. *Appl Catal B* 221:715–725
- Mohd Adnan Mohd A, Julkapli Nurhidayatullaili M, Abd Hamid Sharifah B (2016) Review on  $ZnO$  hybrid photocatalyst: impact on photocatalytic activities of water pollutant degradation. *Rev Inorg Chem* 36:77
- Pirhashemi M, Habibi-Yangjeh A, Rahim Poursan S (2018) Review on the criteria anticipated for the fabrication of highly efficient  $ZnO$ -based visible-light-driven photocatalysts. *J Ind Eng Chem* 62:1–25
- Akyol A, Bayramoglu M (2010) Photocatalytic performance of  $ZnO$  coated tubular reactor. *J Hazard Mater* 180(1):466–473
- Xu S, Wang ZL (2011) One-dimensional  $ZnO$  nanostructures: solution growth and functional properties. *Nano Res* 4(11):1013–1098
- Anjum M, Miandad R, Waqas M, Gehany F, Barakat MA (2019) Remediation of wastewater using various nano-materials. *Arab J Chem* 12(8):4897–4919
- Rahman QI, Ahmad M, Misra SK, Lohani MB (2013) Hexagonal  $ZnO$  nanorods assembled flowers for photocatalytic dye degradation: growth, structural and optical properties. *Superlattices Microstruct* 64:495–506
- Kumar R, Kumar G, Umar A (2013)  $ZnO$  nano-mushrooms for photocatalytic degradation of methyl orange. *Mater Lett* 97:100–103
- Rahman QI, Ahmad M, Misra SK, Lohani M (2013) Effective photocatalytic degradation of rhodamine B dye by  $ZnO$  nanoparticles. *Mater Lett* 91:170–174
- Oxley JD, Prozorov T, Suslick KS (2003) Sonochemistry and sonoluminescence of room-temperature ionic liquids. *J Am Chem Soc* 125(37):11138–11139
- Allaf RM, Hope-Weeks LJ (2014) Synthesis of  $ZnO-CuO$  nanocomposite aerogels by the sol-gel route. *J Nanomater* 2014:160–160

31. Wu J-J, Liu S-C (2002) Low-temperature growth of well-aligned ZnO nanorods by chemical vapor deposition. *Adv Mater* 14(3):215–218
32. Li X, Xu H, Chen Z-S, Chen G (2011) Biosynthesis of nanoparticles by microorganisms and their applications. *J Nanomater* 2011:16
33. Vidya C, Manjunatha C, Chandraprabha M, Rajshekar M, Mal AR (2017) Hazard free green synthesis of ZnO nano-photo-catalyst using *Artocarpus heterophyllus* leaf extract for the degradation of Congo red dye in water treatment applications. *J Environ Chem Eng* 5(4):3172–3180
34. Dobrucka R, Długaszewska J (2016) Biosynthesis and antibacterial activity of ZnO nanoparticles using *Trifolium pratense* flower extract. *Saudi J Biol Sci* 23(4):517–523
35. Ahmed S, Chaudhry SA, Ikram S (2017) A review on biogenic synthesis of ZnO nanoparticles using plant extracts and microbes: a prospect towards green chemistry. *J Photochem Photobiol B Biol* 166:272–284
36. Raja A, Ashokkumar S, Pavithra Marthandam R, Jayachandiran J, Khatiwada CP, Kaviyarasu K, Ganapathi Raman R, Swaminathan M (2018) Eco-friendly preparation of zinc oxide nanoparticles using *Tabernaemontana divaricata* and its photocatalytic and antimicrobial activity. *J Photochem Photobiol B* 181:53–58
37. Sharma D, Sabela MI, Kanchi S, Mdluli PS, Singh G, Stenström TA, Bisetty K (2016) Biosynthesis of ZnO nanoparticles using *Jacaranda mimosifolia* flowers extract: synergistic antibacterial activity and molecular simulated facet specific adsorption studies. *J Photochem Photobiol B* 162:199–207
38. Brehm JU, Winterer M, Hahn H (2006) Synthesis and local structure of doped nanocrystalline zinc oxides. *J Appl Phys* 100(6):064311
39. Bhardwaj R, Singh JP, Chae KH, Goyal N, Gautam S (2018) Electronic and magnetic structure investigation of vanadium doped ZnO nanostructure. *Vacuum* 158:257–262
40. Ebadi M, Zolfaghari MR, Aghaei SS, Zargar M, Shafiei M, Zahiri HS, Noghabi KA (2019) A bio-inspired strategy for the synthesis of zinc oxide nanoparticles (ZnO NPs) using the cell extract of cyanobacterium *Nostoc* sp. EA03: from biological function to toxicity evaluation. *RSC Adv* 9(41):23508–23525
41. Kumari P, Panda PK, Jha E, Kumari K, Nisha K, Mallick MA, Verma SK (2017) Mechanistic insight to ROS and apoptosis regulated cytotoxicity inferred by green synthesized CuO nanoparticles from *Calotropis gigantea* to embryonic zebrafish. *Sci Rep* 7(1):1–17
42. Parhira S, Zhu G-Y, Li T, Liu L, Bai L-P, Jiang Z-H (2016) Inhibition of IKK- $\beta$  by epidioxysterols from the flowers of *Calotropis gigantea* (Niu jiao gua). *Chin Med* 11(1):9
43. El-Seedi HR, Khalifa SA, Taher EA, Farag MA, Saeed A, Gamal M, Hegazy M-EF, Youssef D, Musharraf SG, Alajlani MM (2019) Cardenolides: insights from chemical structure and pharmacological utility. *Pharmacol Res* 141:123–175
44. Ahmed S, Chaudhry SA, Ikram S (2017) A review on biogenic synthesis of ZnO nanoparticles using plant extracts and microbes: a prospect towards green chemistry. *J Photochem Photobiol B* 166:272–284
45. Chakrabarti S, Chaudhuri B, Bhattacharjee S, Das P, Dutta BK (2008) Degradation mechanism and kinetic model for photocatalytic oxidation of PVC–ZnO composite film in presence of a sensitizing dye and UV radiation. *J Hazard Mater* 154(1–3):230–236
46. Akpan UG, Hameed BH (2009) Parameters affecting the photocatalytic degradation of dyes using TiO<sub>2</sub>-based photocatalysts: a review. *J Hazard Mater* 170(2):520–529
47. Khezrianjoo S, Revanasiddappa HD (2013) Photocatalytic degradation of acid yellow 36 using zinc oxide photocatalyst in aqueous media. *J Catal* 2013:1–6
48. Mishra G, Mukhopadhyay M (2019) TiO<sub>2</sub> decorated functionalized halloysite nanotubes (TiO<sub>2</sub>@HNTs) and photocatalytic PVC membranes synthesis, characterization and its application in water treatment. *Sci Rep* 9(1):1–17
49. Akbal F (2005) Photocatalytic degradation of organic dyes in the presence of titanium dioxide under UV and solar light: effect of operational parameters. *Environ Prog* 24(3):317–322

**Publisher's Note** Springer Nature remains neutral with regard to jurisdictional claims in published maps and institutional affiliations.